Section 7

Global and regional climate models, sensitivity and impact experiments, response to external forcing, monthly and seasonal forecasting.

Modeling of a permafrost response to extreme temperature events

M.M. Arzhanov, S.N. Denisov

A.M. Obukhov Institute of Atmospheric Physics RAS, 3, Pyzhevsky, 119017 Moscow, Russia
arzhanov@ifaran.ru

Estimates of contemporary climate changes in the Arctic region are of particular importance due to developing infrastructure. Growing gas and oil exploration on the sea Arctic shelf require an implementation of the growing factor of the global climate change in building strategies for social-economic development in the region. Development of territories of the Arctic region is connected with a risk of environmental damage. Typical aspects of human activity at development of territories can lead to a risk of vegetation damage and removal of snow cover. These factors are important when accounting processes of atmosphere interaction with the underlying surface and subsurface frozen soil. An increase of air temperature in high latitudes of the Northern hemisphere is followed by a growth of cold-season temperature. According to observations on a meteorological station of Salekhard [1], the linear trend of average annual near-surface temperature for 1990-2015 is around 0.03 °C/year (see also [2]). The trends during winter and autumn seasons are 0.04 °C/year and 0.05 °C/year, respectively. The trend for this period in spring is around 0.02-0.03 °C/year. A linear trend of the surface air temperature is not significant in summer. Using these data a time series (25 model years) of the sinusoidal input monthly air temperatures has been prepared to exclude interannual fluctuations (experiment CTL) (fig. 1a).

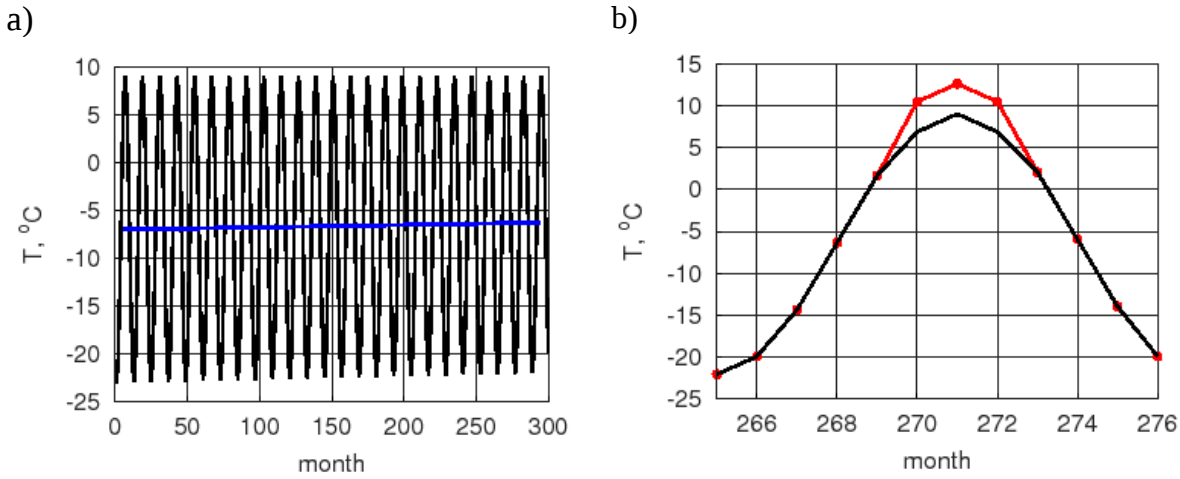

Fig. 1. Input air temperature. (a) Monthly (black) and yearly (blue) mean surface air temperatures for 25 model years (experiment CTL). (b) Monthly mean surface air temperatures in the 23rd model year in CTL (black) and EXT (red).

The increase of global and regional near-surface temperature causes an increase in the number of extreme events, including the periods of extremal high air temperatures. The response of Arctic permafrost to such events is insufficiently studied [3]. The mean summer air temperature in Salekhard was as high as 16.03 °C in 2016, some 3.6 °C above the 1990-2015 average. This is the warmest summer since 1882 when the records started, amounting to an offset of 3 standard deviations from the mean (1990-2015). To take this fact into account, we applied higher input summer temperatures in experiment EXT than those in experiment CTL for the 23rd model year (fig. 1b). For other years, the input air temperatures were the same in both experiments.

The air temperature during the summer period is the main factor of impact on the seasonal thawing of frozen soil. For modeling the impact of extreme air temperatures on the thermal regime of permafrost a heat transfer model was used [4]. To estimate the atmospheric impact on the human-changed permafrost ecosystems of the Arctic regions the vegetation- and snow-less surface were supposed. According to the model estimates for experiment CTL the soil temperature trend at a depth of 0.5 m is 0.03 °C/year for the chosen period. This trend coincides with a trend of input annual mean air temperature. The trend is about 0.02° C/year at a depth of 3 m decreasing by less then 0.02° C/year at a 10 m depth. The difference of the soil temperature in experiments of EXT and CTL is shown in fig. 2.

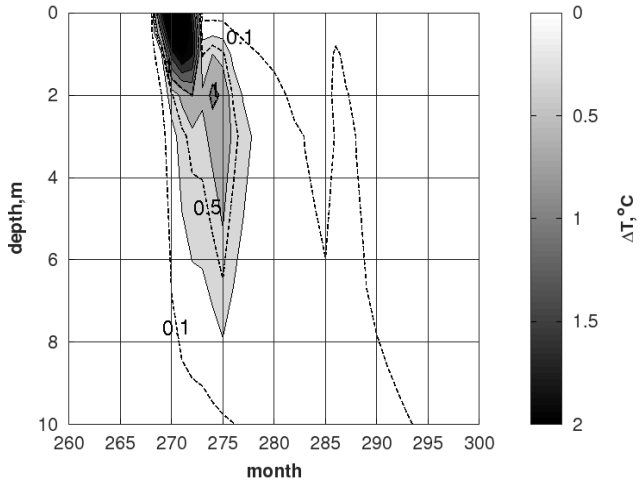

Fig. 2. Soil temperature difference between EXT and CTL experiments.

The main impact of extremal air temperature in EXT compared to CTL is noted near the surface up to 1.7-2.0 m. Though perturbation of the soil temperature field reaches approximately 10 m, at such depths it is insignificant. The largest increase in thaw depth about 6% occurs in summer and autumn. In the next years differences in thaw depth become less. Extreme temperature events can affect the soil temperature field. At the same time, the resulting perturbation is localized near the surface and disappears with time.

Acknowledgments. This work was supported by the Russian Foundation for Basic Research (17-05-00561, 16-07-01205); the Presidium of the Russian Academy of Sciences; the Ministry for Education and Science of the Russian Federation (11.G34.31.0007).

References

1. GISTEMP Team, 2018: GISS Surface Temperature Analysis (GISTEMP). NASA Goddard In stitute for Space Studies. Dataset accessed 2018-05-05 at https://data.giss.nasa.gov/gistemp/.
2. Arzhanov M.M. and I.I. Mokhov. Temperature trends in the permafrost of the Northern Hemisphere: comparison of model calculations with observations // Doklady Earth Sciences. 2013. Vol. 449. Part 1. pp. 319-323.
3. Isaksen K., Benestad R.E., Harris C., and J.L. Sollid. Recent extreme near-surface permafrost temperatures on Svalbard in relation to future climate scenarios // Geophys. Res. Lett. 2007. Vol. 34. p. L17502.
4. Arzhanov M.M., Eliseev A.V., Demchenko P.F., and I. I. Mokhov. Modeling of changes in temperature and hydrological regimes of subsurface permafrost, using the climate data (Reanalysis) (in Russian) // Kriosfera Zemli. 2007. Vol. 11 N.4. pp. 65-69.

Estimations of natural methane fluxes taking into account the wetland area dynamics

Sergey Denisov, Maxim Arzhanov
A.M. Obukhov Institute of Atmospheric Physics, RAS, Moscow, Russia
denisov@ifaran.ru

The natural emission of methane is estimated at 35-50% of the total, the main natural source is wetlands. It is not only the largest source of methane, but also the most volatile on an inter-annual scale. There are concerns that methane emissions from wet ecosystems can grow significantly with climate warming and the inclusion of feedbacks between the climate and the methane cycle.

The annual-mean surface air temperature is expected to increase by 3–5 °C in Siberian region by the end of the 21st century. The largest increase of precipitation rate is expected in winter for all river basins especially in the northeastern part of Eurasia. It can result in changes in the thermal and hydrological regime of soil.

Methane emissions from wetlands were calculated using the model, which takes into account the soil temperature and moisture content and the amount of carbon substrate in soil for the methane production (Denisov et al. 2015). It has been complemented with wetland area calculation scheme based on TOPMODEL (Beven et al., 1979). Main thermophysical characteristics of high latitude soils are obtained using a numerical scheme of heat and moisture transfer in the atmosphere-underlying surface-soil accounting for dynamics of frozen and thaw layers boundaries with water phase changes (Arzhanov et al. 2008, Arzhanov et al. 2012).

An ensemble of 45 realizations of the multi-year data of meteorological variables at the land surface, calculated by the ECHAM5 for different initial and identical boundary conditions for a 34-year period (from 1.01.1979 to 31.12.2012) was specified as space-distributed input data. The initial conditions (the state of the atmosphere for January 1, 1979) were specified as instantaneous atmospheric conditions at various 12 hour intervals in December 1978.

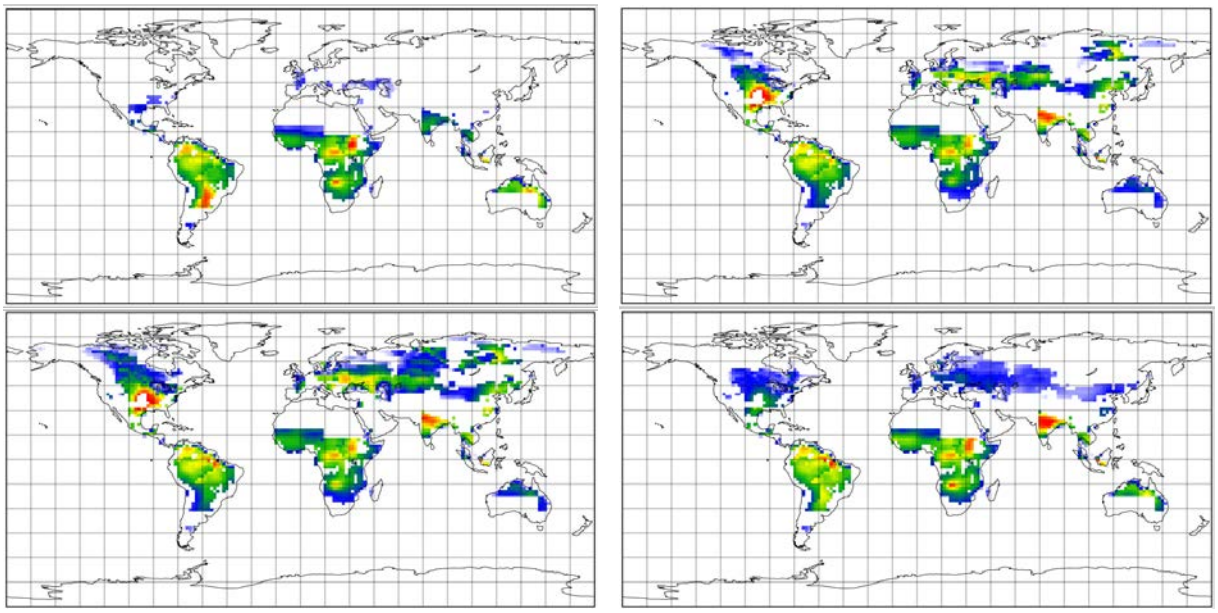

Fig.1 Global methane emissions for January, June, August and October

The ensemble average of annual emissions from Western Siberia over the estimated period equals to 3.8 TgCH4 (uncertainty index is 10%). The highest methane flux estimations (more than 2 TgCH4) were obtained for August-September (Fig. 1). The trend of emissions is about 0.02 TgCH4/yr. Total annual emissions in individual years may differ by a factor of more than 3 between different realizations of the model. For individual months, the uncertainty index of emission mean values is 7-35%, and it is minimal for months with maximal emissions. It is concluded that the uncertainty of methane emission mean values due to climatic noise decreases with the growth of the averaging time interval. The uncertainty of the estimates for the emission mean values on the monthly scale has a pronounced seasonal variability. The uncertainty index of the standard deviation estimates for both annual and monthly emission values is 25-26% and has negligible seasonal variability.

This work is supported by RFBR (16-07-0120, 17-05-00561, 18-05-00087) and Russian Science Foundation (17-77-10152).

References

Arzhanov M.M., Eliseev A.V., Demchenko P.F., Mokhov I.I., and Khon V.Ch. Simulation of Thermal and Hydrological Regimes of Siberian River Watersheds under Permafrost Conditions from Reanalysis Data // Izvestiya, Atmospheric and Oceanic Physics, 2008, Vol. 44, No. 1, pp. 83–89.

Arzhanov M.M., Eliseev A.V., Mokhov I.I. A global climate model based, Bayesian climate projection for northern extra-tropical land areas // Glob. Planet. Change. 2012. V.86- 87. P.57-65.

Denisov S. N., Eliseev A.V., Mokhov I.I., Arzhanov M.M. Model estimates of global and regional atmospheric methane emissions of wetland ecosystems // Izvestiya, Atmospheric and Oceanic Physics, 2015, Vol. 51, No. 5, pp. 482-487.

Beven, K. J. and Kirkby, M. J. A physically based variable contributing area model of catchment hydrology, Hydrol. Sci. Bull., 1979, 24, 43-69.

Precipitation-temperature relationship in spring-summer for Eurasian regions:

Model projections

Mokhov I.I.[1,2], Timazhev A.V.[1]

[1]A.M. Obukhov Institute of Atmospheric Physics RAS
[2]Lomonosov Moscow State University
mokhov@ifaran.ru

Observations since the end of 19th century (Meshcherskaya and Blazhevich, 1997) show a general decrease of precipitation in spring-summer months in mid-latitudinal European and Asian Russian regions under regional warming (Mokhov et al., 2002; Mokhov, 2005). Here we estimate possible changes in the precipitation-temperature relationship in spring-summer months from model simulations for the 21st century for different regions, in particular for three mid-latitudinal regions in the Northern Eurasia (Fig. 1).

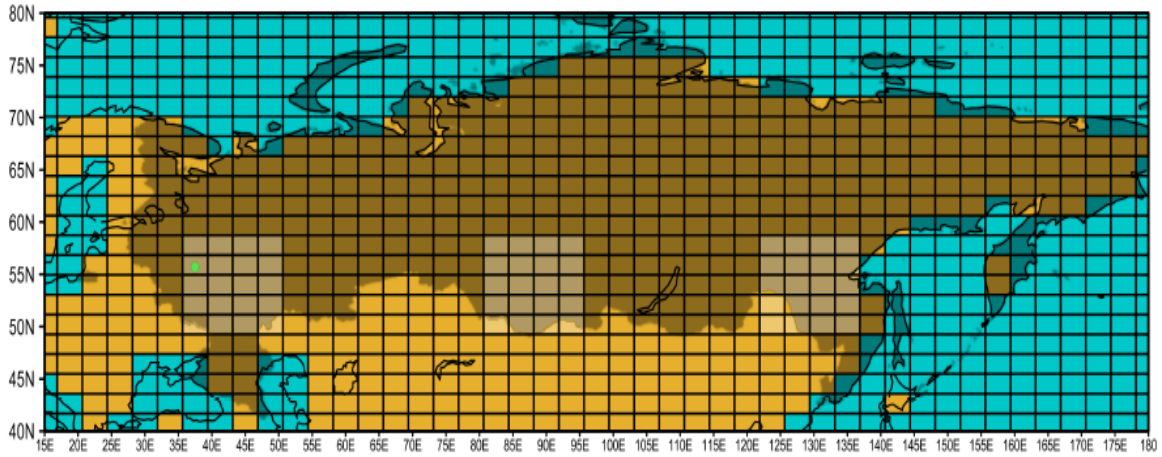

Fig. 1. Selected three regions in midlatitudes of Northern Eurasia.

Figure 2 shows precipitation anomalies in May-July in dependence on corresponding anomalies of surface air temperature for three Eurasian regions (European Territory of Russia (ETR), Asian Territory of Russia (ATR) and Far East of Russia (DVR)) from simulations with the IPSL-CM5B global climate model (Dufresne et al., 2013) under different scenarios. Precipitation and temperature anomalies are analyzed for ETR, ATR, and DVR for 3 scenarios: historical (1850-2005), RCP4.5 and RCP8.5 (2006- 2100) (Fig. 1). Anomalies were calculated for 3 midlatitude regions of Northern Eurasia (Fig. 1).

For historical scenario there is a well-marked negative correlation between temperature and precipitation for ETR and ATR. A significant difference is exhibited for DVR in the field of influence of the Asian monsoon.

Under the warming scenarios in the 21st century, the range of precipitation fluctuations increases and the relationship between precipitation and temperature becomes less significant.

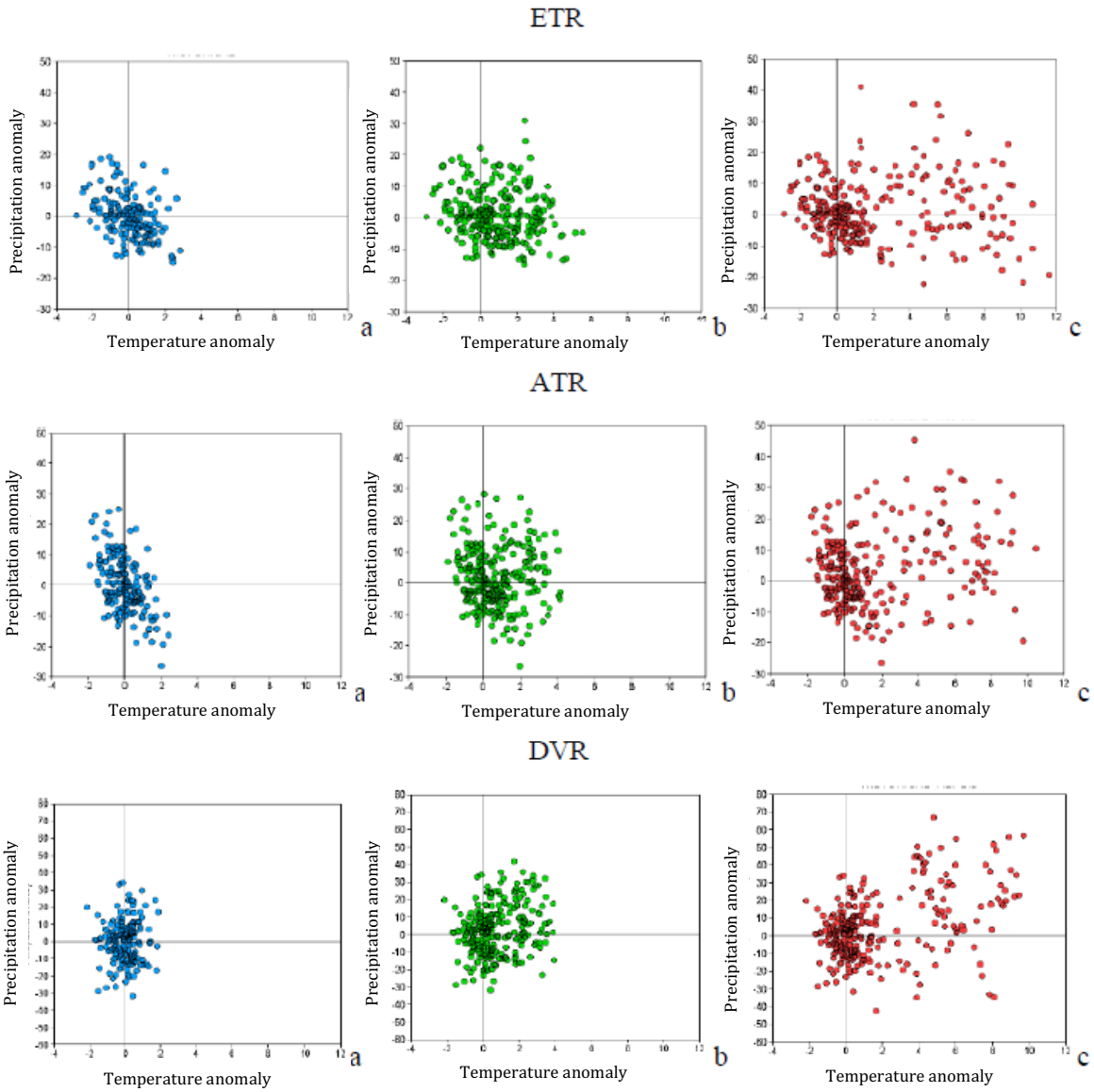

Fig. 2. Precipitation anomalies in May-July in dependence on corresponding anomalies of surface air temperature for three Eurasian regions (ETR, ATR, and DVR) from model simulations for the period 1850-2005 ("historical" scenario (a)) and for the period 1850-2100 ("historical" and RCP4.5 (b), "historical" and RCP8.5 (c)).

This work was supported by the RFBR and RAS.

References

Dufresne J.L. *et al*. Climate change projections using the IPSL-CM5 Earth System Model: from CMIP3 to CMIP5. *Clim. Dyn.*, 2013, **40**(9-10), 2123-2165.

Meshcherskaya A.V., Blazhevich V.G. The drought and excessive moisture indices in a historical perspective in the principal grain-producing regions of the Former Soviet Union. *J. Climate*, 1997, **10**, 2670–2682.

Mokhov I.I. Spring-summer climate extremes in Eurasian midlatitudinal regions. *Res. Activ. Atmos. Ocean. Modell.* J. Cote (ed.). Geneva: World Climate Research Programme. WMO TD-No.1276, 2005, 2.7-2.8.

Mokhov I.I., Dufresne J.-L., Khon V.C., Le Treut H., Tikhonov V.A. Regional regimes with drought and extreme wet conditions: Possible changes in XXI century from IPSL-CM2 simulations. *Res. Activ. Atmos. Ocean. Modell.*, WMO/TD-No. 1105, 2002, 07.31–07.32.

Numerical simulation of permafrost thermal structure in West Siberia

M.R. Parfenova[1], M.M. Arzhanov[1], A.V. Eliseev[1,2,3], I.I. Mokhov[1,2]

[1]A.M. Obukhov Institute of Atmospheric Physics RAS
[2]Lomonosov Moscow State University
[3]Kazan Federal University

parfenova@ifaran.ru

Permafrost strongly influences the processes that contribute significantly to both local and global climate on different time scales. In this study, the model for thermal and hydrolocal processes in the soil interior, the Deep Soil Simulator (DSS) [Arzhanov et al., 2007] is used to simulate numerically the evolution of permafrost soils in West Siberia over the last 200,000 years. The DSS is forced by the Climer-2 output as reported by Ganopolsi et al. [2016]. The results of the DSS simulations are compared to the data from the borehole drillings in the respective regions, and also to the results of another numerical simulations of the temperature field for the north of West Siberia [Chuvilin et al., 2013]. Despite the differences in degrees C, the geothermal gradients of simulation results agree well with those of the boreholes data.

For numerical simulations with DSS, the model of permafrost heat transfer mechanisms is used with respect to freezing-thawing cycles. This model was developed at IAP RAS, is based on the solution of the Stefan problem with several water-ice phase transitions boundaries [Arzhanov et al., 2007]. The upper boundary of the simulated area is taken land surface level or the snow cover level (if any), with boundary condition of the first kind established on it -- the near-surface temperature of the CLIMBER-2 data. A geothermal flow of 0.06 W/m^2 is set at the lowest boundary of the simulated area, which is at the depth of 1500 meters.

The results of simulations are temperature distributions in soils in the West Siberia and China. According to the simulations, the geothermal gradients for the selected area are 2.45 C/100 m and 2.53 C/100 m for different longitudes 47-57 N and 57-67 N respectively, at latitudes 90-120 E.

In order to verify how adequate the CLIMBER-2 model reproduces the temperature regime of the soil of West Siberia region, the results were compared to the instrumental data of borehole drilling for present time (Fig. 1). Temperature measurement were obtained from several boreholes in West Siberia at least 200 meters deep.

The geothermal gradients of instrumentally obtained data are 1.741 K/100 m at the location 55.17 N, 82.83 E [https://www.ncdc.noaa.gov/paleo/study/1000884]; 2.784 K/100 m at the location 49.08 N, 114.25 E [https://www.ncdc.noaa.gov/paleo/study/1000765]; 3.767 K/100 m at the location 37.88 N, 92.25 E [https://www.ncdc.noaa.gov/paleo/study/1001031]; 0.709 K/100 m at the location 66.42 N, 112.5 E [https://www.ncdc.noaa.gov/paleo/study/1000881]. The geothermal gradients calculated based on the results of CLIMBER-2 simulations fall within the range of the geothermal gradients of observational data.

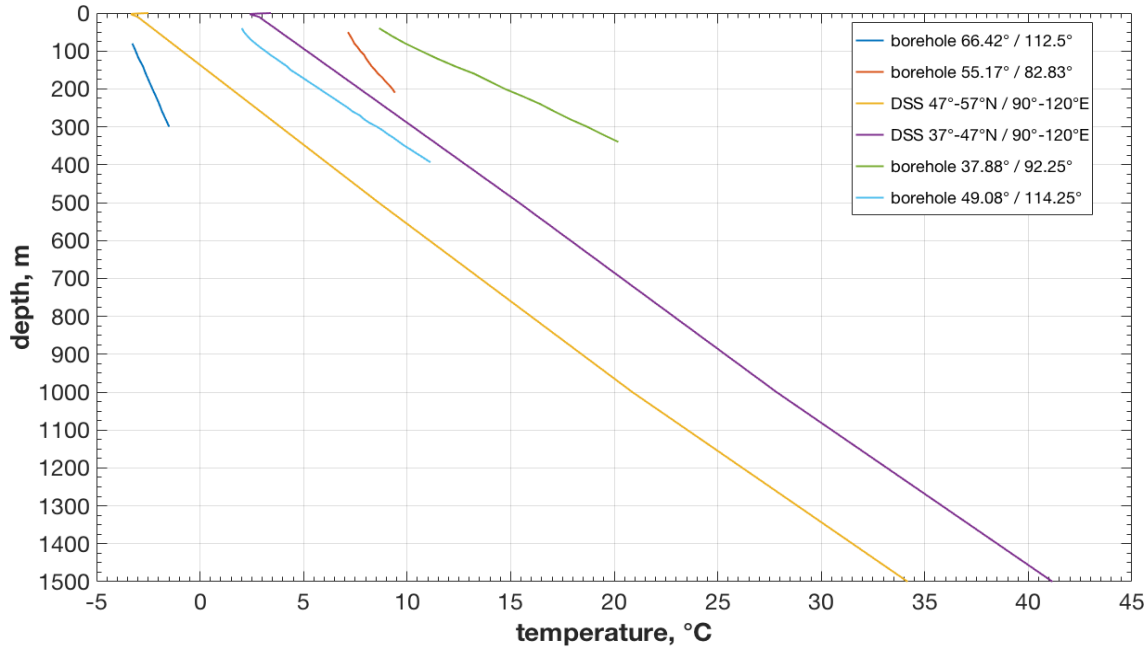

Fig. 1. Soil temperature profiles in West Siberia and China from the DSS simulations and borehole data.

Another comparison of the obtained DSS estimates with the results of numerical simulations of the temperature field for the north of Western Siberia [Chuvilin et al., 2013] illustrates that the model reproduces well a decrease in soil temperature during periods of glacial peaks, in particular about 200,000 years ago and in LGM (about 20,000 years ago), as well as an increase in temperature during the interglacial periods - the Eemian interglacial (120,000 years ago) and the Holocene optimum (from 10,000 years ago). The obtained values of the temperature at 1500 m for the current period are 34-42 C, which agrees well with the estimates of 35-45 C from [Chuvilin et al., 2013].

References

Arzhanov M.M, Demchenko P.F., Eliseev A.V., Mokhov I.I. 2008. Simulation of Characteristics of Thermal and Hydrologic Soil Regimes in Equilibrium Numerical Experiments with a Climate Model of Intermediate Complexity // Izvestiya, Atmospheric and Oceanic Physics, Vol. 44, No. 5, pp. 548–566.

Chuvilin E., Tumskoy V., Tipenko G. et al. 2013. Relic gas hydrate and possibility of their existence in permafrost within the South-Tambey Gas Field // Conference proceedings SPE 166925. SPE Arctic and Extreme environments, p. 1–9.

Ganopolski A., Winkelmann R., Schellnhuber H.J. 2016. Critical insolation-CO_2 relation for diagnosing past and future glacial inception // Nature, v. 529, no. 7585, pp. 200-203.

Huang, S., Pollack, H.N., and Shen, P.Y. 2000. Temperature trends over the past five centuries reconstructed from borehole temperatures // Nature, 403, pp. 756-758. doi: 10.1038/35001556.

The 206-day lunar cycle of temperature anomalies in 2016/17

Nikolay S. Sidorenkov* and Ian R.G.Wilson**
* Hydrometeorological Research Center of the Russian Federation, Moscow
**The Liverpool Plains Daytime Astronomy Centre, Curlewis, NSW, Australia
sidorenkov@mecom.ru

The spring of 2017 presented an unusual surprise in the development of weather processes in the European territory of Russia (ETR). As early as the second week of February, the air temperature rose to freezing, and in March the average daily temperature became positive. On March 1, in many cities of the ETR, the absolute maximum temperatures were above average with values more like those expected for the middle of April. There was a rapid melting of the snow cover. Much earlier than normal, the rivers Don, Oka, Dnieper, Zapadnaya Dvina, Volga were opened for navigation.

By the second week of April, the temperature rise was reversed and the resulting negative temperature anomalies persisted until the last days of April. After a four-day wave of summer-like heat, starting on May 4th, the temperature returned to the cooler values of April. In the third week of May, the temperature began to return to more normal values. However, in the first days of June, a wave of cold Arctic air again invaded, bringing temperatures closer to the extremely low values experience earlier in the year. In many areas of ETR in June, there were still frosts.

Now let us consider more closely the evolution of the temperature anomalies in the ETR using data from the weather station of the VDNKh (Moscow). Fig. 1 shows the anomalies in the average daily temperature over 2016/17. The daily data are smoothed by calculating their moving averages over 27 days values. The smoothed data are represented by a thick curve. The graphs of temperature in the cities of Samara, Krasnodar and Rostov on Don have the same appearance as in Moscow.

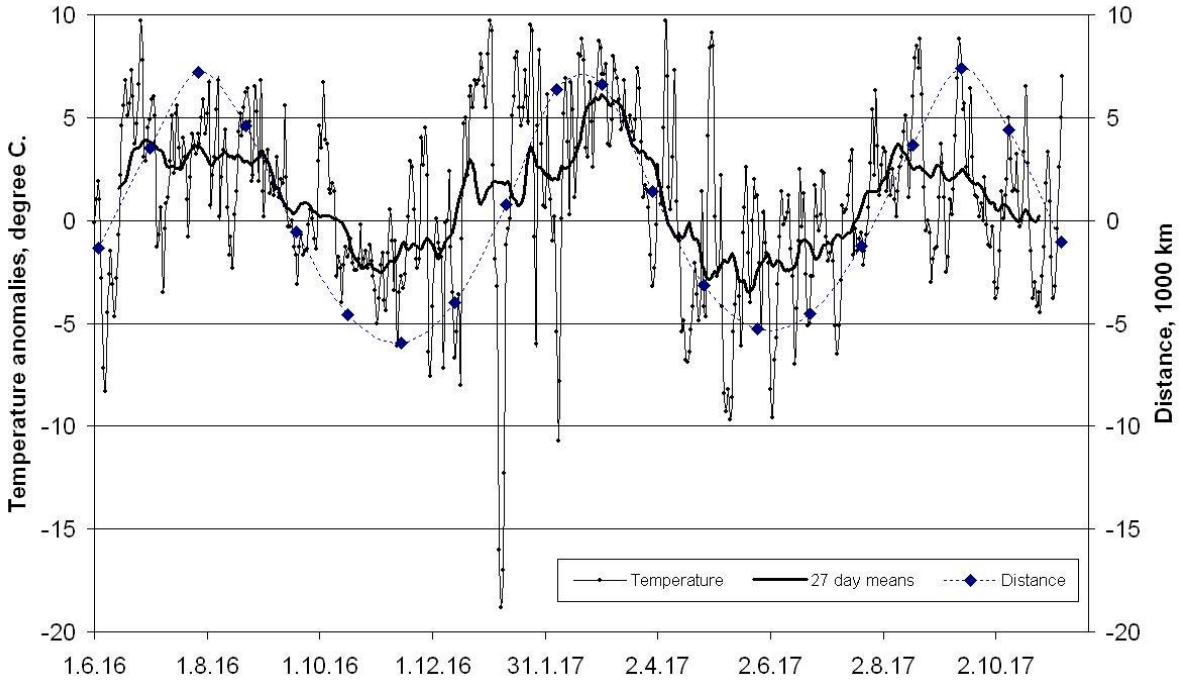

Figure 1. Deviation of the perigee distance of the Moon from 362464 km. (Rhombuses) and the course of anomalies in the average daily air temperature in Moscow in 2016/17 (a thin curve - the average daily values, a thick curve - moving average for 27 days values).

In Fig. 1 the smoothed curve exhibits a distinct sinusoidal-like wave, with minimums in November 2016 and June 2017 and maximums in July 2016, March and September 2017. The swing of the temperature anomaly fluctuations reaches 10 degrees, and the period (the time interval between the minima) is about 205 days. This period is almost precisely the same as the 206-day period that we obtained in the periodogram for the 43-year-old series of temperature anomalies for Moscow [2, 3]. The 206-day cycle is well known to astronomers as being half of the Full Moon Cycle of 411.78 days. From the physical point of view, the cycle of 206 days is the period of the beating of the frequencies of the anomalistic (27.55 days) and the synodic (29.53 days) months [Sidorenkov, 2015], or the synodic month and the evection period of the lunar orbit (31.81 days).

The perigee end of the line-of-apse of the lunar orbit is continuously shifting from west to east (i.e. in a pro- grade direction) in the sky, returning to roughly the same position with respect to the stars once every 8.85 year. As a direct consequence of this pro-grade movement, if the Perigee end of the lunar line-of-apse starts out points directly at the Sun, it will take another 1.127 years or 411.8 days before it returns to pointing at the Sun again. This true because:

$$\frac{1}{1} - \frac{1}{8.85} = \frac{1}{1.127}$$

This means that Perigee end of the lunar orbit will go from pointing directly at the Sun, to pointing directly away from the Sun once every 206 days.

In addition, the distance between the Moon and the Earth the magnitude of perigee also varies from 370,000 km to 356,000 km over the same period of 206 days. This phenomenon is illustrated in Fig. 1, where diamonds are marked by deviations of perigee distances from their average value of 362,464 km, and their dynamics are represented by a dashed curve. The duration of the lunar anomalistic month (that is, the time interval between two consecutive passages of the moon through the perigee) also changes with a period of 206 days from 28.5 to 24.8 days.

The Earth in its motion around the barycentr of the Earth- Moon system reflects all the movements of the Moon on a scale of 1:81. Therefore, the Earth has similar variations of the pericentric distance and the angular velocity of the monthly circulation around the Earth-Moon barycenter with a period of 206 days. [2, 3]. The 206-day cyclicity of the monthly movement of the Earth is reflected in processes in the earth's shells, primarily in the hydrosphere [1] and the atmosphere.

The 206-day temperature anomaly cycle leads to violations of seasonal temperature variations. For example, due to its contribution, the 2016 winter over European Russia began nearly one month earlier, while the 2017 summer set in one month later than its usual time. As a result, the "top" of the summer shifted to August, and the fall, to the end of September.

References

1. Avsuk Yu.N., Maslov L.A. Long Period Tidal Force Variations and Regularities in Orbital Motion of the Earth-Moon Binary Planet System //Earth, Moon, and Planets, 2011. Vol. **108**, Issue 1. pp 77-85. DOI 10.1007/s11038-011-9381-8.

2. N.S. Sidorenkov, 2009: The interaction between Earth’s rotation and geophysical processes. WILEY-VCH Verlag GmbH & Co. KGaA, Weinheim, 2009.

3. Sidorenkov N. S.. Celestial Mechanical Causes of Weather and Climate Change. //Izvestiya, Atmospheric and Oceanic Physics, 2016, Vol. 52, No. 7, pp. 667–682. © Pleiades Publishing, Ltd., 2016. DOI: 10.1134/S0001433816070094

Spring tides in the atmosphere

Nikolay S. Sidorenkov and Kseniya Sumerova
Hydrometeorological Research Center of the Russian Federation, Moscow
sidorenkov@mecom.ru

The years 2016/2017 marked the most striking manifestation of 206-day lunar cycles in weather over European Russia. The smoothed air temperature anomalies followed the variations in the perigee distance (that is, the distance between the Moon and the Earth at times when the Moon is at the nearest point to the Earth, i.e., at the perigee), which represents a sinusoid with a period of 206 days [2].

The 206-day cyclicity results from beats produced by interference of close frequencies of the anomalistic month (27.55 days between two successive perigees) and the synodic month (29.53 days between two successive new moons). This phenomenon is easy to observe by comparing the durations of full moons and new moons [3] or by keeping track of variations in the height of spring tides, i.e., tides at syzygies (at times of new and full moons) [1].

The main feature of spring tides is that the curve for each syzygy is well approximated by a sinusoid (beat envelope) with a period of 412 days, and their phases differ by 180° (Fig. 1). Therefore, for any tidal characteristic, every positive anomaly at one syzygy corresponds to a negative anomaly at the next syzygy. The cause is that the orbit of the Moon is elliptic. If a full moon coincides in time with perigee, the distance from the Moon to the Earth is reduced to the minimum and the tidal force becomes maximum (positive anomalies). Roughly in a half-month, at a new moon, the Moon reaches an opposite point of the orbit, i.e., it is at the maximum distance from the Earth (near apogee) and the tidal force becomes minimum (negative anomalies). In 27.55 days, the Moon returns to the perigee, but it happens two days earlier than full moon. Next time, it returns four days earlier, and so on. With every lunar revolution, the tidal force decreases at full moon and increases at new moon and, after 3.5 synodic months, the spring tides at full and new moon become of equal size (at a beat node) and then the tidal force at new moon dominates that at full moon, reaching the maximum range (at a antinodes or crest) after 7 synodic months. Next, the range again decreases up to the next node, which occurs in 3.5 months, and so on. A change in the sign of the anomalies from full to new moons and back always happens at beat nodes in 206 days.

The appearance of a 206-day cycle in the 2017 weather prompted our study of spring tides in the atmosphere, which should be exhibited in oscillations of atmospheric pressure in a similar manner to the spring tides in Fig. 1 [1]. Specifically, a series of three-hour ground-surface pressure measured at the VDNKh weather station in Moscow over the last two years was used to calculate daily mean pressure values and their anomalies. The daily pressures at the Moscow State University meteorological observatory averaged over 1966–2010 were used as normals [4].

Next, for each full moon day, we chose the daily mean pressure anomaly over this day. A series of atmospheric pressure anomalies for all new moons was separately generated in a similar manner. With the help of Excel, the atmospheric pressure anomalies at the VDNKh weather station were plotted for full moons (open circles on the red curve) and for new moons (solid circles) over 2016–2017 (Fig. 2).

Figure 2 shows that the spring oscillations of atmospheric pressure are highly noisy as compared with the spring sea tides (Fig. 1). Nevertheless, we can observe the basic features of the atmospheric spring tides, namely, nodes (in the summer of 2016 and May of 2017) and antinodes (in February–March and September–October of 2017). It can be seen that the pressure anomalies at new and full moons are of different signs. The pressure anomalies at full and new moons can be approximated by sinusoids with beat envelope periods of about 412 days and with opposite phases. The range of the oscillations at antinodes reaches 40 mb, which is comparable in order of magnitude with spring tides in the ocean [1].

Thus, Fig. 2 suggests that the geodynamical forces in 2016/2017 were able to overcome the stochastic thermodynamics of the atmosphere and imposed their celestial-mechanical tidal rhythm on the weather evolution and the variations in pressure and temperature in Moscow. The striking manifestation of a 206-day lunar cycle in the 2016/2017 weather in Moscow was associated with spring tides in the atmosphere. The 206-day cycle of spring tides violated the normal seasonal variations in meteorological characteristics and led to numerous local record measurements of daily weather parameters over European Russia in 2016/2017.

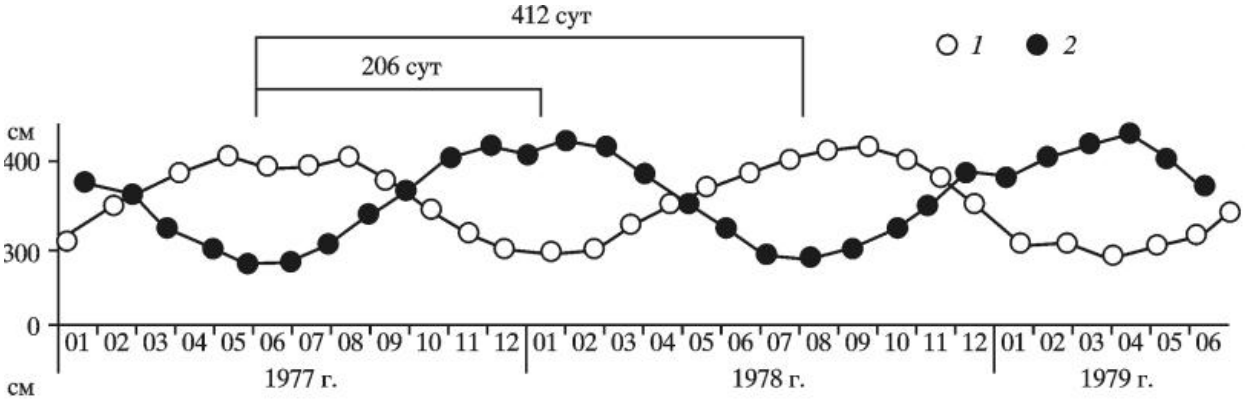

Fig. 1. Spring tides in Murmansk over 1977–1979: (*1*) full moon and (*2*) new moon.

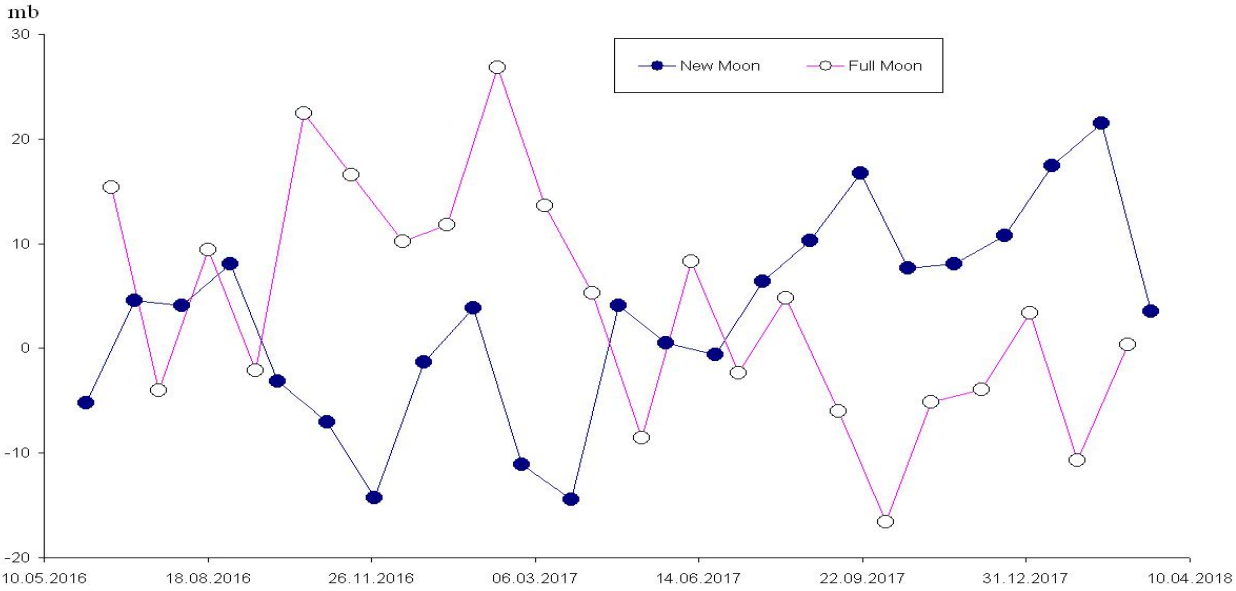

Fig. 2. Spring oscillations of the atmospheric pressure measured at the VDNKh weather station over 2016/2017.

References

1. Avsuk Yu.N., Maslov L.A. Long Period Tidal Force Variations and Regularities in Orbital Motion of the Earth-Moon Binary Planet System //Earth, Moon, and Planets, 2011. Vol. **108**, Issue 1. pp 77-85. DOI 10.1007/s11038-011-9381-8.

2. Sidorenkov N.S., Wilson I.R.G. The 206-day lunar cycle of temperature anomalies in 2016/17 . // CAS/JSC WGNE Research Activities in Atmospheric and Oceanic Modelling, submitted

3. Sidorenkov N. S.. Celestial Mechanical Causes of Weather and Climate Change. //Izvestiya, Atmospheric and Oceanic Physics, 2016, Vol. 52, No. 7, pp. 667–682. © Pleiades Publishing, Ltd., 2016. DOI: 10.1134/S0001433816070094

4. Sidorenkov N. S., Isaev A.A., et al. Thin structure of time variations of atmospheric pressure. //Poceedings of Hydrometcenter of Russia. – 2008. – Vol. 342, – P. 177-186. (in Russian)